

3.6 SIMULATION OF FALL AND WINTER SURFACE ENERGY BALANCE OVER A DENSE URBAN AREA USING THE TEB SCHEME

Grégoire Pigeon^{*1}, Mark A. Mosicki², James A. Voogt² and Valéry Masson¹

¹CNRM-GAME, Météo France-CNRS, Toulouse, France

²UNIVERSITY OF WESTERN ONTARIO, LONDON, ON, CANADA

1 INTRODUCTION

Modelling of the urban climate has become of great interest for several reasons. Urban climates impact the majority of the world's population, so they are strategic topics of research. For example, during the 2003 heat wave in Europe, the urban heat island (UHI) strengthened the heat stress conditions in large cities like Paris. Finally, the prospect of large scale climate change calls for an adaptation of urban areas to the future environment (Best 2006; Hallegatte et al. 2007). A large number of models, using different approaches, have been developed recently to reproduce the processes that govern urban climate (for a review see Masson, 2006). But beyond this first step of development, only a few models have been extensively evaluated against field measurements of fluxes and surface temperatures (Grimmond and Oke 1999a; Masson et al. 2002; Lemonsu et al. 2004; Hamdi and Schayes 2005).

The Town Energy Balance (TEB) model (Masson 2000) is a single-layer urban canopy model (Masson 2006). It represents the urban surface by a simplified set of urban canyons of all possible directions and is forced by atmospheric data provided either by observations (offline mode) or by an atmospheric model (coupled mode). It has been designed to be easily transferable from research applications to numerical weather prediction systems or climate models. TEB has been evaluated against field data sets in a light industrial area (Masson et al. 2002) of Vancouver and dense urban areas of Mexico City (Masson et al. 2002), Marseille (Lemonsu et al. 2004; Roberts et al. 2006) and Łódź (Offerle et al. 2005). These evaluations show that TEB is able to reproduce well the exchanges of heat and momentum between the urban surface and the atmosphere. One limitation of TEB evaluation is that the measurement period is restricted to summer conditions for the studies of Masson et al. (2002), Lemonsu et al. (2004) and Roberts et al. (2006). In this study, our objective is to conduct an evaluation of TEB for fall and winter over a dense urban area of Toulouse, where micrometeorological measurements were conducted during the CAPITOUL field program (Masson et al. 2008). For the first time in this study, the parameterization of the anthropogenic heat releases is evaluated against an inventory of energy consumption. The paper first presents the methods adopted for this evaluation including the characteristics of the studied area, and the observation and simulation strategies. Then, the

evaluation of the different fluxes (net radiation, sensible and anthropogenic heat flux) and the surface temperature of each facet are presented.

2 METHODS

The evaluation is conducted following the same methods as in Masson et al. 2002 and in Lemonsu et al. 2004. In this mode, TEB computes energy fluxes for the urban fraction and ISBA (Interaction Soil–Biosphere–Atmosphere model, Noilhan and Planton 1989) for the other types of surface cover. The simulations were performed in an offline mode; that is the model is not coupled with an atmospheric mesoscale model but instead the atmospheric forcing is given by observations above the canopy layer (average over 30 min periods). This mode of running TEB reduces errors due to the atmospheric forcing and makes it possible to run long term simulations. TEB has been run for two periods during which Q_F has a strong contribution: a fall period from 15 October to 15 November 2004 and then a winter period from 15 January to 15 February 2005. This evaluation strategy was incorporated in the design of the CAPITOUL field program: all the variables necessary to run and evaluate TEB were measured in a dense urban area of the old centre of Toulouse (Masson et al. 2008; Pigeon et al. 2007). The urbanisation around the surface energy balance station is very homogeneous. The model is run with inputs that characterize the surface conditions over a 500 m radius circle around the tower. This area includes the turbulent and radiative source areas for the measurements evaluated in this study.

2.1 STUDY AREA

The study area is located in the old centre of Toulouse where measurements were conducted during the CAPITOUL field program (Masson et al. 2008). In this neighbourhood, vegetation is very scarce (8%, Table 1) and buildings are typically 4–5 stories. The area is classified as Urban Climate Zone 2 (UCZ2) according to Oke (2006). The quantification of the urban parameters of this area is presented in Table 1. Values are averages over the 500-m radius circle around the surface energy balance station. Parameters were estimated from the Geographical Information System of Toulouse which is composed of a three dimensional vector database of the buildings and aerial ortho-rectified photography at a 0.25m resolution. Buildings in the centre of Toulouse are very homogeneous and most of them are from the 19th

* Corresponding author address: Grégoire Pigeon, CNRM-GAME, Météo France-CNRS, Toulouse, France. E-mail : gregoire.pigeon@meteo.fr

century. For that reason, walls are built with bricks and most are not insulated as well as the roofs. Most roofs are covered with tiles (constructed from the same clay material as the bricks). The thermal and radiative characteristics of the walls, roads and roofs are presented in Table 2.

Table 1: Characteristics of the area

Parameter	Value
Building pad ¹	0.54
Road pad	0.38
Tree pad	0.06
Grass pad	0.02
Building height (m)	14.9
Aspect ratio	1.4

¹ Plan area density

² ratio between the height of the building and the width of the street

2.2 MEASUREMENTS

The forcing parameters (for details on the instrumentation see Pigeon et al. 2007; Masson et al. 2008) were measured at the top of a pneumatic tower installed on a building roof, 20m above street level. For comparison with the outputs of TEB, the fluxes of net radiation (Q^*) and the sensible heat (Q_H) were also measured at the top of the tower, which was in the inertial layer. Surface temperatures are state variables of the TEB model. For that reason, their evaluation is of great interest and they are among the parameters that could be estimated with satellites and assimilated by TEB. TEB computes separate energy budgets for the road, the roof and the wall. For each of these structures, a mean surface temperature is computed. In TEB computations, all the directions for the urban canyon are considered and surface temperatures are averaged over all these directions. As surface temperatures strongly depend on the orientation of the streets and its geometry, it is important that measurements constitute a representative sample of all the possible directions and geometries. In CAPITOUL, three streets, between which the azimuth varies by 60 degrees, have been instrumented (Table 3) with infra-red thermometers (IRT). In each street, three IRTs were installed to measure the surface temperature of the two walls and the road. The roof surface temperature was measured for a single tile roof. The IRT was set up two meters above the top of the roof so that both sides of the roof are in its field of view (FOV). In order to make meaningful comparisons between measurements and the model, the raw data have undergone four processing steps. First, the sensors were calibrated with a black-body. Second, a data correction for emissivity was needed and was calculated assuming a one reflection event between the road and the walls. Emissivity values for the walls of the canyons were estimated by using a weighted average based on the types of building material making up the entire surface of the wall under study. Third, for road and wall

surface temperatures, a weighting procedure was applied to take into account (i) the variable geometry (canyon aspect ratio) of the study canyons and (ii) the canyon orientations. This weighting procedure is intended to provide an appropriately averaged wall and road temperature for comparison with the TEB output, which assumes any canyon orientation is possible with equal probability (Masson 2000) for a single specified canyon aspect ratio. It provides improvements to the model evaluation statistics of up to 0.3 C compared to the use of an arithmetic weighting scheme (Moscicki 2007). For the road surface temperatures, a fourth processing step has been applied because vehicles passed through the field of view of the IRTs. Depending on the traffic intensity, the corrections are up to a few tenths of a degree. These four processing steps of the raw IRT data are presented with more details in Pigeon et al., 2008.

2.3 ESTIMATION OF ANTHROPOGENIC HEAT

TEB takes into account three sources of anthropogenic heat (Q_F): releases from traffic, releases from industry, and releases from space heating. The first two sources of Q_F need to be prescribed in TEB as additional sensible or latent flux sources. The central area of Toulouse presented in this study is free of industrial activities. Traffic releases over the 500-m radius circle area around the instrumented tower have been estimated using traffic counts from two automatic counters located on two major roads of the area (for more details on the methodology see Pigeon et al. 2007). With these data, a mean annual traffic heat release of 8 W m⁻² was computed for the area. The other releases from buildings were estimated with an inventory of energy consumption measured at a 100m resolution over the entire agglomeration of Toulouse for the period of the CAPITOUL field campaign (Pigeon et al. 2007). These deliveries of energy are supposed to instantaneously compensate heat loss from the buildings as in Ichinose et al. (1999) and Sailor and Lu (2006). This inventory was built on the real consumption of electricity and gas which represent 90% of the energy use in Toulouse buildings. For the other sources of energy (domestic fuel, wood and others), mean annual values from 2001 were available. Over the area presented in this study, releases from buildings have been shown to be the dominant component of Q_F during fall and winter (Pigeon et al. 2007). In TEB, to mimic space heating, a fixed minimum internal building temperature of 292 K is specified (Masson 2000; Masson et al. 2002). This parameterization has never been evaluated before this study. Hence, a new diagnostic has been computed in the model to estimate the additional heat flux associated with this parameterization. The anthropogenic heat flux associated with space heating, noted Q_{Fsh} , is estimated, using the following equation, as a weighted average of the heat fluxes between the building

interior and the internal layer of the wall and between the building interior and the internal layer of the roof when the internal temperature is set to its minimum value of 292 K :

$$Q_{Fsh} = \frac{S_{wall} \frac{1}{R_i} (T_{imin} - T_{iw}) + S_{roof} \frac{1}{R_i} (T_{imin} - T_{ir})}{S_T}, \text{ where}$$

Q_{Fsh} is the anthropogenic heat flux associated with space heating ($W m^{-2}$), S_{wall} is the area of the wall, S_{roof} is the area of the roof, T_{imin} is the minimum building internal temperature, T_{iw} is the internal wall layer temperature, T_{ir} is the internal roof layer temperature, R_i is the aerodynamic resistance for the inside of the building equal to $0.123 K m^2 W^{-1}$ (Masson et al. 2002) and S_T is the total area of the canyon. For comparison with the inventory of energy consumption, this flux has been averaged over daily periods.

3 RESULTS

Mean diurnal cycles of net radiation, sensible heat flux, anthropogenic heating and surface temperatures of the wall, the roof and road are presented for fall and winter respectively in Figures 1 and 3. Scatter plots of the same measured and modelled variables are presented in Figures 2 and 4 for fall and winter respectively. Bias and Root Mean Square Difference (RMSD) scores are computed for the same parameters for the same seasons.

3.1 FALL PERIOD

During fall, the behaviour of the model is very good for Q^* . The mean daily cycle (Figure 1, top left graph) is very well reproduced and the variability of the model and the observations are comparable. It results in a very low scatter of the model predictions compared to the observations (Figure 2, top left graph) as well as a small bias and a RMSD lower than $10 W m^{-2}$ (Table 4). Since downward radiation fluxes are used to force the model in this study, this result demonstrates the performance of TEB in representing the radiation trapping in the canyon and the surface temperatures. The wall surface temperature is the best reproduced temperature with bias and RMSD lower than 1K (Table 4). The daily cycle is also well predicted (Figure 1, middle right graph) and the representation of the model estimates as a function of the observations shows little scatter (Figure 2, middle right graph). The roof surface temperature is also well simulated by the model even if it is slightly overestimated during the day (Figure 1, bottom left graph) or more generally for the highest values (Figure 2, bottom left graph). The road surface temperature is slightly underestimated by the model by 1.5K on average (Table 4). This underestimation is larger during the night than during the day (Figure 1, bottom right graph). The lowest road surface temperatures are underestimated by the model while

the highest temperatures are generally well reproduced in the simulation (Figure 2, bottom right graph). The ensemble average daily cycle of Q_H over the period (Figure 1, top right) is very well represented by the model and only a small negative bias of the model computed for this flux (Table 4) is noted. On Figure 1, the Q_F estimates for the model (middle left graph) are the superposition of the mean value of the heat releases associated with space heating during the period and the heat releases associated with traffic. Concerning the estimates of Q_F calculated from the inventory of energy consumption, the ensemble average daily cycle is presented. On Figure 2, the scatter plot of the daily average fluxes are represented and it can be seen that the model has a tendency to be too dynamic compared to the observations (middle left graph) under-predicting the lowest values and over-predicting the highest Q_F values. Nevertheless, the important result here is the good reproduction by the model of the mean value of Q_F with a difference between both averages of $1 W m^{-2}$ (Table 5). To conclude, for the evaluation of TEB during the fall, it is important to note its ability to reproduce the specific observed characteristics of the urban energy balance such as the slightly positive sensible heat flux during the night period that is probably associated with a strong contribution of the heat releases associated with space heating.

3.2 WINTER PERIOD

During winter, TEB still reproduces a very good Q^* . This is the case for its ensemble average daily cycle (Figure 3, top left graph) and also for most of the samples during this period as can be seen on the scatter plot between the model and the observations (Figure 4, top left graph). It results in a RMSD for this flux that is still lower than $10 W m^{-2}$ (Table 4). This result is still associated with a generally good ability of the model to reproduce the surface temperatures, especially the wall surface temperature for which there is a very low RMSD between the model and the observations (Table 4), as well as a good ensemble average daily cycle (Figure 3, middle right graph). However, it can be seen that TEB has a tendency to underestimate the road temperature by slightly more than 2K (Table 4). Figure 4 (bottom right graph) shows that this underestimation is more accentuated for the lowest values of the road surface temperature. On the other hand, the magnitude of the daily cycle is, on average, well reproduced (Figure 3, bottom right graph). At the same time, the model has a slight tendency to predict higher roof surface temperatures than those observed (Figure 3, bottom left graph). This is the case during the middle of the day and it certainly results in the slight overestimation of Q_H by the model for the same hours (Figure 3, top right graph). The model also has a tendency to predict slightly larger values of Q_H during the night hours and the releases associated with the space heating are generally too high (Figure 3, middle left graph and

Table 4). This behavior of the model is particularly true for the highest values of Q_F (Fig. 4, middle left graph). Despite these differences between the model and the observations, TEB is generally able to reproduce the order of magnitude of this term during winter (approximately 80 W m^{-2}) and the processes associated with this term: building surface temperatures higher than air temperature and positive heat flux during night periods.

4 CONCLUSIONS

In this study an evaluation of the TEB model has been performed for fall and winter time periods against the CAPITOUL field data set collected over Toulouse. The model has been run in an offline mode forced by the meteorological observations measured at the top of a tower in the dense old centre of Toulouse. The evaluation has been conducted against the energy fluxes measured at the top of the same tower and the surface temperatures measured with infra-red thermometers for a selected set of walls, roads and roofs with different orientations and aspect ratios. For the two periods of study, the model reproduces well the most important characteristic of the urban surface energy balance: the strong contribution of sensible heat flux with small positive values during the night associated with high values of the anthropogenic heat flux. This last point is important since this study is the first attempt to evaluate the TEB parameterization of the space heating against an inventory of energy consumption built with a high spatial and temporal resolution over the agglomeration of Toulouse. It will be interesting to test, when TEB is coupled to a three dimensional atmospheric model, if the ability of the urban scheme to reproduce strong anthropogenic heat releases and positive values of the sensible heat flux during the night can lead to the reproduction of typical nocturnal urban boundary layer structures like the crossover of vertical profiles of air temperature (Oke, 1987) in comparison to a rural profile. Another interesting application of the ability of TEB to correctly reproduce the anthropogenic heat releases is the possibility to use it for the forecast of the energy demand for space heating at the scale of a city.

5 REFERENCES

- ASHRAE, 1989, ASHRAE Handbook: 1989 Fundamentals. ASHRAE, 797 pp
- Best, M.J., 2006, Progress towards better weather forecasts for city dwellers: from short range to climate change. *Theor. Appl. Climatol.*, 84, 47–55
- Grimmond CSB, Oke TR, 1999a, Heat storage in urban areas: observations and evaluation of a simple model. *J. Appl. Meteorol.* 38, 922–40
- Hallegatte S, Hourcade J, Ambrosi P, 2007, Using climate analogues for assessing climate change economic impacts in urban areas. *Clim Change*, 82, 47–60
- Hamdi R, Schayes G, 2005, Validation of the Martilli's urban boundary layer scheme with measurements of two mid-latitude European cities. *Atmos Chem Phys Dis*, 5, 4257–89
- Ichinose T, Shimodono K, Hanaki K, 1999, Impact of anthropogenic heat on urban climate in Tokyo. *Atmos Environ*, 33, 3897–909
- Lemonsu A, Grimmond CSB, Masson V, 2004 Modelling the surface energy balance of an old Mediterranean city core. *J Appl Meteorol*, 43, 312–27
- Masson V, 2000, A physically-based scheme for the urban energy budget in atmospheric models. *Bound Layer Meteorol*, 94, 357–97
- Masson V, 2006, Urban surface modelling and the meso-scale impact of cities. *Theor Appl Climatol*, 84, 35–45
- Masson V, Grimmond CSB, Oke TR, 2002, Evaluation of the Town Energy Balance (TEB) scheme with direct measurements from dry districts in two cities. *J Appl Meteorol*, 41, 1011–26
- Masson V, Gomes L, Pigeon G, Lioussé, K, Lagouarde JP, Voogt JA, Salmond JA, Oke TR, Legain D, Garrouste O, 2008, The Canopy and Aerosol Particles Interactions in TOulouse Urban Layer (CAPITOUL) experiment. *Meteorol Appl Phys*, In press.
- Moscicki MA, 2007, A comparison of modelled and observed urban surface temperatures in Toulouse, France. Unpublished M.Sc. Thesis, The University of Western Ontario, London, ON, Canada, 171 pp
- Noilhan J, Planton S, 1989, A simple parameterization of land surface processes for meteorological models. *Mon Wea Rev*, 117, 536–49
- Offerle B, Grimmond CSB, Fortuniak K, 2005, Heat storage and anthropogenic heat flux in relation to the energy balance of a central European city centre. *Int J Climatol*, 25, 1405–19
- Oke TR, 1987, Boundary layer climates, 2nd edn. Methuen, New York and London
- Oke TR, 2006, Towards better scientific communication in urban climate. *Theor Appl Climatol*, 84, 179–90
- Pigeon G, Legain D, Durand P, Masson V, 2007, Anthropogenic heat release in an old European agglomeration (Toulouse, France). *Int J Climatol*, 27, 1969–81
- Roberts SM, Oke TR, Grimmond CSB, Voogt JA, 2006, Comparison of four methods to estimate urban heat storage. *J Appl Meteorol Climatol*, 45, 1766–81
- Sailor DJ, Lu L, 2006, A top-down methodology for developing diurnal and seasonal anthropogenic heating profiles for urban areas. *Atmos Environ*, 38, 2737–48

Table 2: Characteristics of the wall, the roof and the road taken in the model.

	Surface albedo α	Surface emissivity ϵ	Layer	Depth (m)	Material	Heat Capacity ($10^6 \text{ J m}^{-3} \text{ K}^{-1}$)	Thermal conductivity ($\text{W m}^{-1} \text{ K}^{-1}$)
WALL	0.25	0.92	1	0.01	red bricks	1.58	1.15
			2	0.05			
			3	0.18			
			4	0.05			
			5	0.01			
ROOF	0.15	0.90	1	0.01	red tiles	1.58	1.15
			2	0.05			
			3	0.02	wood	2.20	0.20
			4	0.01			
ROAD	0.08	0.95	1	0.01	asphalt	1.74	0.82
			2	0.04			
			3	0.20	aggregate	2.00	2.1
			4	1.00	Gravel and soil	1.40	0.4

Table 3: Characteristics of the streets instrumented during the CAPITOU field campaign

Road	Azimuth ($^{\circ}$ /North)	Mean Aspect ratio	Road sky view factor	Wall view ¹	% brick	% concrete	% glass	Weighted emissivity	Wall sky view factor
Alsace	0	1.4	0.309	270	80	0	20	0.932	0.237
				90	0	50	50	0.895	
Pomme	120	1.8	0.231	210	50	0	50	0.935	0.188
				30	80	0	20	0.932	
Rémusat	60	1.8	0.276	150	20	50	30	0.893	0.229
				330	60	0	40	0.934	0.205

¹direction to which the wall is pointing ($^{\circ}$ /North)

Table 4: Bias and RMSD between the model and the observations for the two simulation periods.

		Q^* (W m^{-2})	Q_H (W m^{-2})	Q_F (W m^{-2})	T_s WALL (K)	T_s ROOF (K)	T_s ROAD (K)
Fall (15/10-15/11)	bias	4	-11	2	0.8	1.0	-1.4
	RMSD	8	44	23	0.9	2.1	1.6
Winter (15/01-15/02)	bias	5	16	18	0.0	1.2	-2.2
	RMSD	7	52	28	0.5	2.2	2.4

Table 5: Comparison between estimates of the anthropogenic heat flux in the observations and in the model

	Q_F (W m ⁻²) Observations	Q_F (W m ⁻²) Simulation
Fall (15/10/04-15/11/04)	46	47
Winter (15/01/05-15/02/05)	71	90

Figure 1: Ensemble average daily cycle of net radiation (top left), sensible heat flux (top right), anthropogenic heat flux (middle left), wall surface temperature (middle right), roof surface temperature (bottom left) and road surface temperature (bottom right) for the fall period simulation. Standard deviations are represented by grey shaded area (observations) and error bars (model)

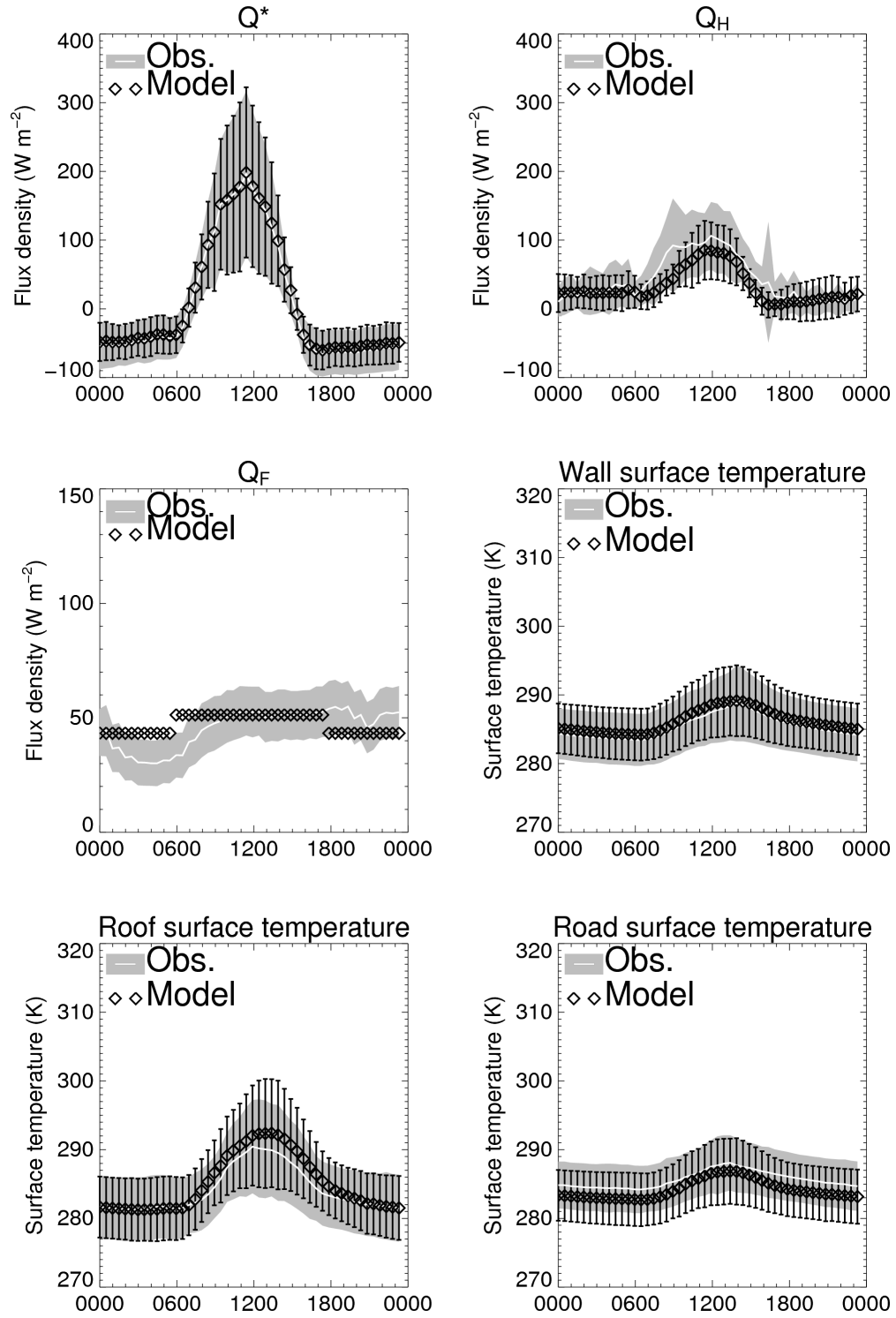


Figure 2: Scatter plots of model predictions versus observations of net radiation (top left), sensible heat flux (top right), anthropogenic heat flux (middle left), wall surface temperature (middle right), roof surface temperature (bottom left) and road surface temperature (bottom right) for the fall period simulation

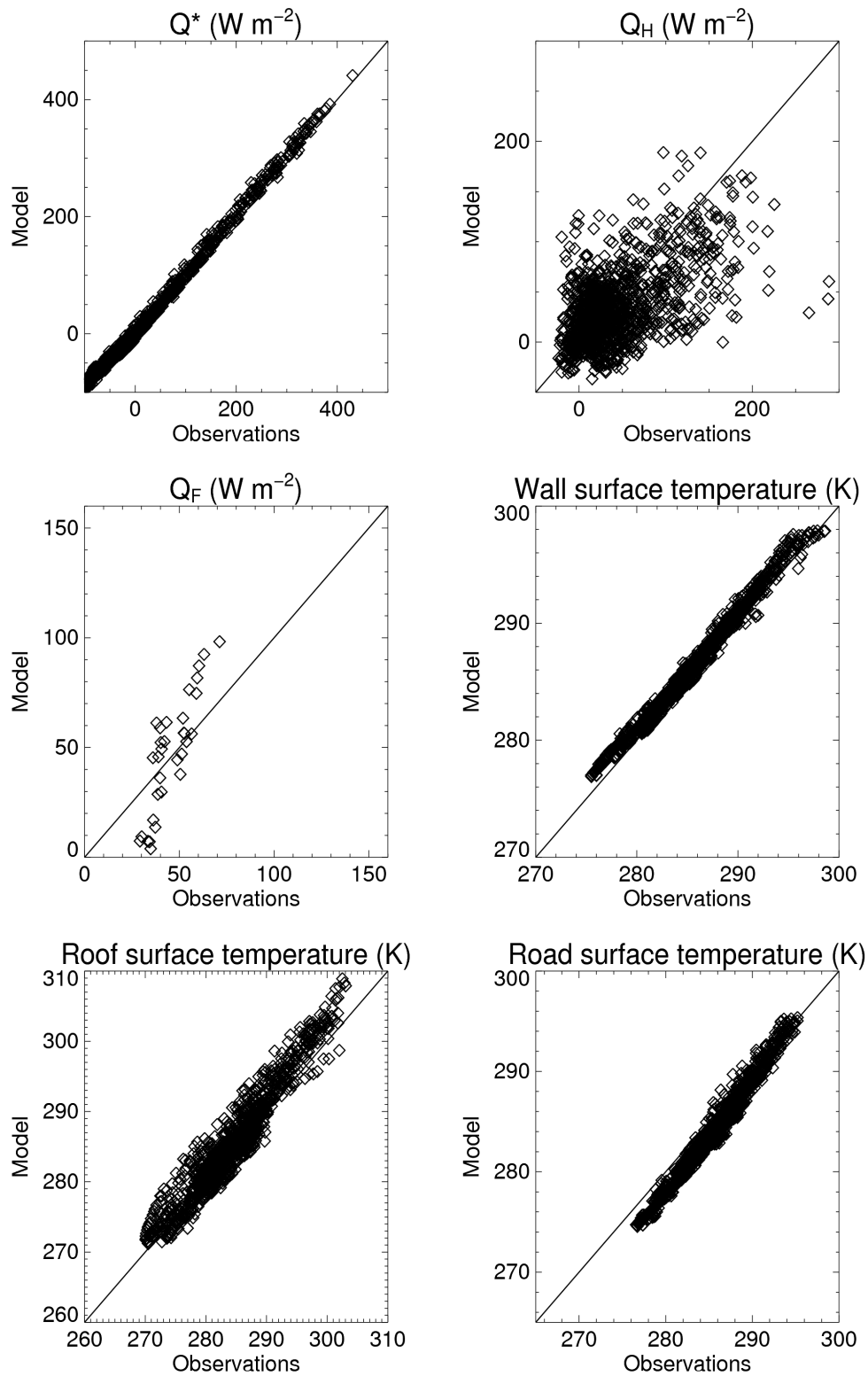


Figure 3: Ensemble average daily cycle of net radiation (top left), sensible heat flux (top right), anthropogenic heat flux (middle left), wall surface temperature (middle right), roof surface temperature (bottom left) and road surface temperature (bottom right) for the winter period simulation. Standard deviations are represented by grey shaded area (observations) and error bars (model)

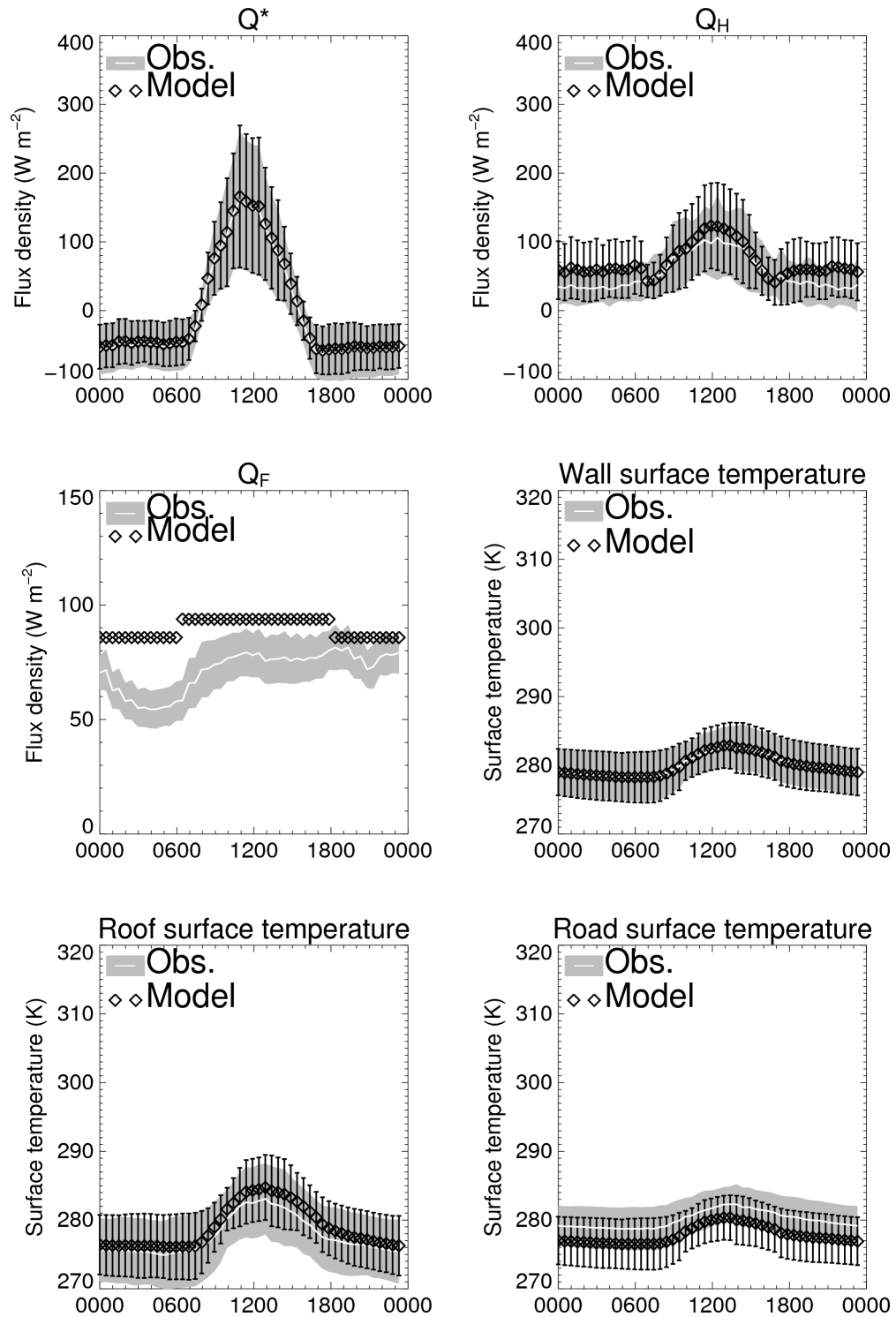


Figure 4: Scatter plots of model predictions versus observations of net radiation (top left), sensible heat flux (top right), anthropogenic heat flux (middle left), wall surface temperature (middle right), roof surface temperature (bottom left) and road surface temperature (bottom right) for the winter period simulation

